Lithuanian Journal of Physics, Vol. **56**, No. 2, pp. 79–85 (2016)
© Lietuvos mokslų akademija, 2016

THEORETICAL STUDY OF α- AND γ-V_2O_5 DOUBLE-WALLED NANOTUBES

V.V. Porsev, A.V. Bandura, and R.A. Evarestov

St. Petersburg State University, 7/9 Universitetskaya nab., 199034 St. Petersburg, Russia

E-mail: v.porsev@spbu.ru

Received 4 October 2015; accepted 21 June 2016

The first-principles calculations of the atomic and electronic structure of double-walled nanotubes (DWNTs) of γ-V_2O_5 have been performed and the obtained properties have been compared with those of α-V_2O_5 ones. The DWNT structure relaxation leads to the formation of two types of local regions: (1) adhesion regions and (2) puckering regions. Although the structure of adhesion regions of α-V_2O_5 DWNTs is close to the structure of bulk α-V_2O_5, this is not the case for γ-V_2O_5 DWNTs. The resulting structure of adhesion regions in γ-V_2O_5 SWNTs allows us to assume the existence of hypothetical stable phases, with one of them resembling the experimentally observed R-Nb_2O_5 and $(V_{0.7}Mo_{0.3})_2O_5$ crystals.

Keywords: vanadium pentoxide, nanotubes, DFT

PACS: 61.43.Bn, 61.46.Np

1. Introduction

Vanadium pentoxide is the subject of intensive theoretical and experimental investigations due to its numerous industrial applications. It forms a great number of various nanostructures which are promising materials for implementing them in Li-ion battery [1] and supercapacitor technologies [2] as chemical actuators [3] and field-emission devices [4]. Nanocables which consist of carbon nanotubes (CNT) covered with ultrathin V_2O_5 layers are the examples of vanadium pentoxide nanostructures [2, 5]. The atomic structure of V_2O_5 layers in such CNT–V_2O_5 nanocomposites is very close to the structure of bulk V_2O_5 [2].

In Ref. [5] the interactions between the CNT surface and the V_2O_5 layer are assumed as weak van der Waals forces, so the oxide layer can be considered as a V_2O_5 nanotube with the atomic structure derived from the bulk V_2O_5. The properties of nanotubes can strongly differ from those of the bulk and films and require careful investigation [6]. For example, an improvement in the catalytic properties of V_2O_5 single-wall nanotubes (SWNTs) with respect to the single layer was found by means of computational modelling of the catalytic oxidation of carbon monoxide [7].

Along with the most stable α-V_2O_5 phase there exists the metastable γ-V_2O_5 (or γ'-V_2O_5 as designated in some articles) [8]. The γ-V_2O_5 attracts the current attention as the Li-ion cathode material [9] or nanostructured catalyst [10]. According to our previous calculations [11, 12], the bulk γ-V_2O_5 is less stable than the bulk α-V_2O_5, however, the α- and γ-V_2O_5 layers and SWNTs are energetically equivalent.

In most cases, the observed vanadium pentoxide nanotubes are multi-walled. In our previous work [13] we investigated the atomic and electronic structure of DWNTs obtained from the α-V_2O_5 phase. Here we present the results of the study of γ-V_2O_5 DWNTs and compare them with those of α-V_2O_5 ones.

2. Computational details

The hybrid DFT – Hartree–Fock method with the PBE0 exchange–correlation functional [14, 15] was used. Computations were performed using a Gaussian atomic basis set implemented in the CRYSTAL09 computer code [16, 17]. We used a full electron consistent portable basis set of the triple-zeta valence with the polarization quality, pob-TZVP [18] for O and V atoms. The empirical Grimme correction (PBE0-D) [19] was applied to take into account the dispersion interaction. The results obtained for the bulk V_2O_5 using the Grimme correction agree well with the experimental data [20]. The scaling factor s_6 is set to 0.5 according to [21], whereas the steepness d and the cutoff radius R_{cut} for direct lattice summation are set equal to 20 and

25.0 Å, respectively. Brillouin zone (BZ) integration was performed over 12 **k**-points chosen according to the Monkhorst–Pack scheme [22]. The lattice parameters and atomic positions of all considered structures were fully optimized. Relaxations were performed until the forces on atoms were less than 0.015 eV·Å^{-1}.

3. Properties of bulk crystals, single layers, and SWNTs of α- and γ-V_2O_5

The space group of α- and γ-V_2O_5 is *Pmmn* (59) [23, 24] and *Pnma* (62) [25], respectively (Figs. 1, 2 and Table 1). Both phases consist of layers stacked in the [001] direction and bound by van der Waals interaction between the vanadyl oxygen and vanadium of the next layer. These layers consist of edge and corner shared tetragonal pyramids VO_5 forming zigzag chains in the [010] direction. Directions of vanadyl bonds in the layers are alternate in the [100] direction as "up-up-down-down" and "up-down-up-down" for α- and γ-V_2O_5, respectively. It should be noted that the layers in the bulk γ-V_2O_5 are not simply stacked one over each other as it occurs in the bulk α-V_2O_5. Every second layer in γ-V_2O_5 is rotated by 180° around the [001] direction. Thus, only the next nearest layers are translationally invariant in contrast to α-V_2O_5.

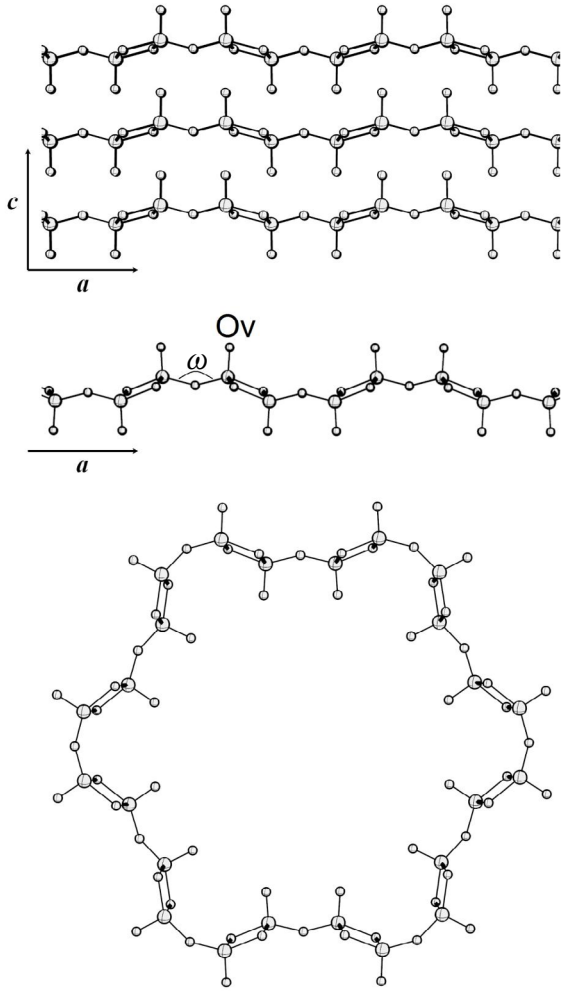

Fig. 1. The structures of bulk crystal (upper), single layer (middle) and (6,0) SWNT (bottom) of α-V_2O_5. The vanadyl oxygen atoms Ov and bridging V-O-V angles ω are shown at the single layer as an example. V, large balls; O, small balls.

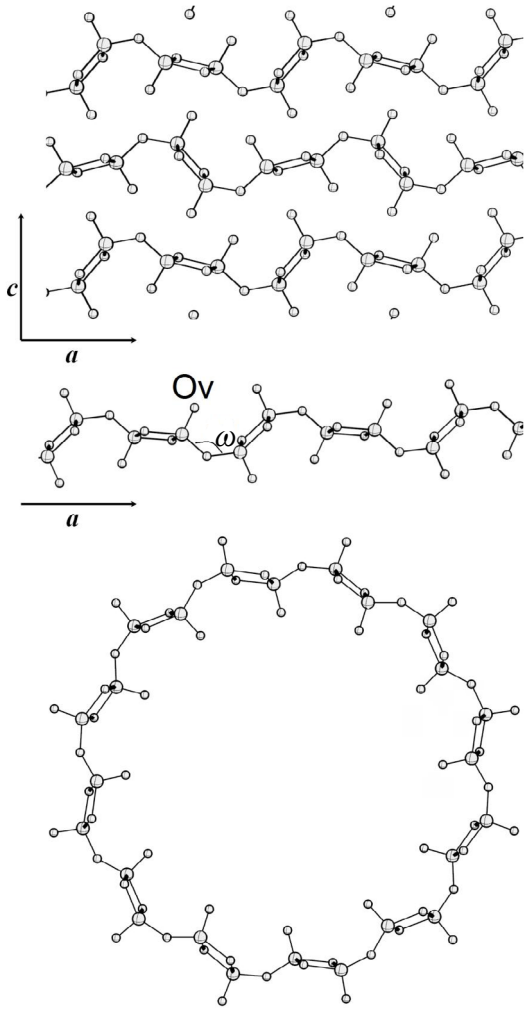

Fig. 2. The structures of bulk crystal (upper), single layer (middle) and (6,0) SWNT (bottom) of γ-V_2O_5. The vanadyl oxygen atoms Ov and bridging V-O-V angles ω are shown at the single layer as an example. V, large balls; O, small balls.

The V_2O_5 single layers are cut from the bulk crystal parallel to the (001) plane. Their layer groups are *Pmmn* (46) and $P2_1/m11$ (15) for α- and γ-V_2O_5, respectively [11]. Due to the layered structure of V_2O_5 bulk phases the structure of single layers undergoes only minor changes during the segregation from the bulk.

Rolling up of these layers results in the formation of SWNTs. Layers of both phases are characterized by the simple rectangular lattice that imposes

Table 1. Properties of bulk crystals, single layers and SWNTs of α- and γ-V_2O_5.

	D[1], Å	t[1], Å	E_{form}[2], kJ/mol	E_{str}[2], kJ/mol
α-V_2O_5, *Pmmn* (59)				
Bulk	–	–[3]	0	–
Single layer	∞	–[3]	42	0
SWNT (3,0)	10.3	3.52	52	10
SWNT (4,0)	13.2	3.53	44	3
SWNT (6,0)	19.8	3.54	43	1
SWNT (8,0)	27.7	3.54	43	1
SWNT (9,0)	31.3	3.54	43	1
SWNT (12,0)	42.3	3.54	43	1
γ-V_2O_5, *Pmna* (62)				
Bulk	–	–[4]	11	–
Single layer	∞	–[4]	41	0
SWNT (3,0)	10.2	3.54	42	1
SWNT (4,0)	13.8	3.54	41	0
SWNT (6,0)	20.9	3.54	42	1
SWNT (8,0)	28.1	3.54	42	1
SWNT (9,0)	31.7	3.54	43	2
SWNT (12,0)	39.9	3.54	42	1

[1] D is the average diameter of nanotube estimated as the sum of radial distances to outmost and innermost oxygen atoms, t is the translational period.

[2] E_{form} is the formation energy and E_{str} is the strain energy of SWNT.

[3] The optimized (and experimental [23]) lattice parameters of bulk α-V_2O_5 are a = 11.51 (11.54) Å, b = 3.54 (3.57) Å, c = 4.30 (4.38) Å. The optimized lattice parameters of α-V_2O_5 single layer are a = 11.20 Å, b = 3.54 Å.

[4] The optimized (and experimental [25]) lattice parameters of bulk γ-V_2O_5 are a = 10.00 (9.95) Å, b = 3.55 (3.59) Å, c = 9.94 (10.04) Å. The optimized lattice parameters of γ-V_2O_5 single layer are a = 10.24 Å, b = 3.54 Å.

a restriction on the chirality indices of nanotubes in order to provide translational periodicity. Only (n,0) and (0,n) chiralities are possible in this case [6]. We found previously [12] that (0,n) chiralities are less favourable due to bending of stiff zigzag chains. At the same time, the layers of α- and γ-V_2O_5 phases can be easily folded into (n,0) SWNT with the strain energy close to zero. Moreover, the formation energies of (n,0) SWNT are very close for both phases.

4. Properties of V_2O_5 DWNTs

The V_2O_5 DWNTs have been constructed by the coaxial insertion of the narrower SWNT into the wider one. The difference between the radii of inner and outer walls can be obtained by calculating the difference between chirality indices

$$\Delta r = \frac{a \cdot n_{out}}{2\pi} - \frac{a \cdot n_{inn}}{2\pi} = \frac{a \cdot \Delta n}{2\pi}, \quad (1)$$

where a is the single layer cell parameter along the folding direction; n_{out} and n_{inn} are the chirality indices of outer and inner walls.

The Ov (see Figs. 1 and 2) atoms of the SWNTs are directed outward and inward, and the difference in the chirality indices has to be sufficient to avoid Ov atoms from being too close in both walls. The DWNTs with Δn = 3 and 4 have been selected for our research, assuming that a further increase of Δn would not influence the result because walls for Δn > 4 can be considered to be independent.

The second criterion used to choose the DWNTs is their symmetry. To reduce computational costs, the walls are selected in such a way that the symmetry of the DWNTs was as high as possible. This is achieved when we choose SWNTs with the maximal greatest common divisor of the chirality indices. Finally, for our study, we selected the DWNTs (3,0)@(6,0) and (6,0)@(9,0) and the DWNTs (4,0)@(8,0) and (8,0)@(12,0) for Δn = 3 and 4, respectively.

Two possible ways exist for constructing DWNTs in the case of γ-V_2O_5. In order to simulate the structure of the γ-V_2O_5 bulk one of the walls must be rotated by 180° around the axis which lies in the plane perpendicular to the nanotube. The second way is constructing DWNTs without such rotation. We designate DWNTs with and without the layer rotation as γ- and γ^*-DWNTs, respectively.

The interaction between the walls results in the reduction of the inter-wall distance and the formation of local adhesion regions in all considered DWNTs. While the length of an outer wall is constant, the formation of puckering regions with separated walls is observed as well. It should be noted that during geometry optimization no consolidation of two walls into one thick wall is observed, in contrast to TiO_2 DWNTs [21].

In the α-DWNTs the structure of adhesion regions is similar to the structure of the bulk α-V_2O_5 [13] (Fig. 3). Thus, in tubular vanadium pentoxide nanoobjects, we can identify areas of the atomic structure of bulk α-V_2O_5, and this fact agrees well with the experimental observations [26].

Adhesion regions are also found in the optimized structures of γ- and γ^*-DWNTs (Fig. 4). However, the local structure of these regions is different from the structure of bulk γ-V_2O_5 even in the case of γ-DWNT. Moreover, γ-DWNTs with different Δn exhibit different structure of adhesion regions. DWNTs with Δn = 3 reveal the adhesion regions with bridging V-O-V angles ω close to 180°. This angle value differs from the ω angles of 128° or 131° in the γ-V_2O_5 bulk or single layer, respectively. In the case of Δn = 4, the ω angles of adhesion regions are similar to those in the bulk

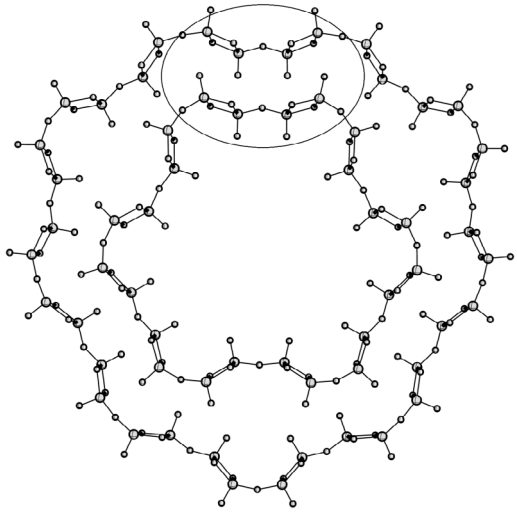

Fig. 3. The structure of $(n_1,0)@(n_2,0)$ α-DWNT with $n_1 = 6$, $n_2 = 9$. The circle indicates one of the adhesion regions. The other adhesion regions in the DWNT are symmetrically equivalent to that marked. V, large balls; O, small balls.

or single layer. The ω angles in the adhesion regions of γ^*-DWNTs are close to 180° for both considered Δn.

The interaction between walls can be characterized by the difference between the energy of DWNT and the sum of energies of the constituent non-interacting SWNTs:

$$E_{\text{int}} = \frac{E\{(n_1,0)@(n_2,0)\} - E\{(n_1,0)\} - E\{(n_2,0)\}}{Z(\text{DWNT})}. \quad (2)$$

Here $E\{(n_1,0)@(n_2,0)\}$, $E\{(n_1,0)\}$ and $E\{(n_2,0)\}$ are the energies of the DWNT and two SWNT constituents, and Z(DWNT) is the number of formula units in the DWNT unit cell. Maximal interaction energy is attributed to the double layer which can be formally considered as DWNT with the infinite radius and perfect stacking of layers on top of each other. DWNTs are less stable than the double layer due to the non-zero curvature and non-perfect stacking.

Formation energies of all considered DWNTs are close and fall in the interval from 27 to 34 kJ/mol. Certain values of the formation energy depend on some particular features of the local atomic structure of DWNT, such as the number of contacts between walls in adhesion regions and the curvature of walls in puckering regions.

5. New phases derived from the structure of adhesion regions of γ- and γ^*-DWNTs

The structure of adhesion regions in γ-SWNTs allows us to assume the existence of stable V_2O_5 phases other than α and γ. The main difference of these hypothetical phases from γ-V_2O_5 is the structure of the single layer in which the ω angle is constrained to 180°. We have designated such a layer as the γ^*-layer. It is easy to show that straightening of the ω angle leads to transformation of the simple rectangular lattice of the layer into a centered rectangular lattice. The corresponding layer symmetry group is $C2/m11$ (18). The calculation of phonons for the γ^*-layer yields the well-defined real frequencies at the Γ-point and one frequency close to zero (the soft-mode phonon) at the R-point of BZ, which indicates the possibility of the reconstruction with cell doubling and transformation of this hypothetical γ^*-layer to the γ-V_2O_5 single layer.

Simple stacking of the γ^*-layers with placing one on top of another results in the centered monoclinic $C2/m$ (12) γ^*-V_2O_5 bulk phase (Fig. 5, right side, and Table 3).

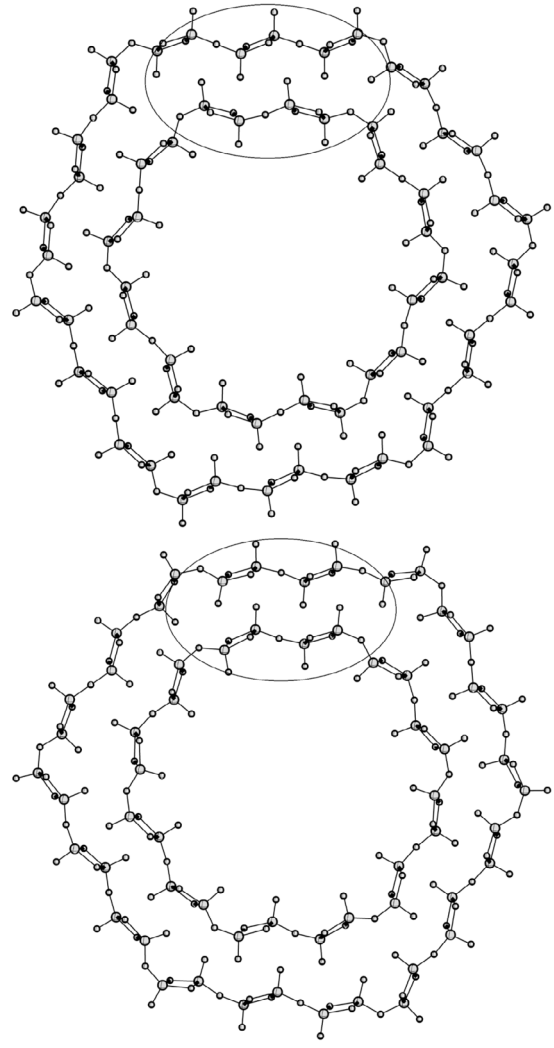

Fig. 4. The structures of $(n_1,0)@(n_2,0)$ γ- and γ^*-DWNT with $n_1 = 6$, $n_2 = 9$ at upper and bottom parts, respectively. Circles indicate one of the adhesion regions. The other adhesion regions in the DWNTs are symmetrically equivalent to those marked. V, large balls; O, small balls.

Table 2. Properties of double layers and DWNTs of α-V_2O_5 and γ- and γ^*-DWNTs.

	D(in)[1], Å	D(out)[1], Å	t[1], Å	E_{form}[2], kJ/mol	E_{int}[2], kJ/mol
α-V_2O_5, *Pmmn* (59)					
Double layer	∞	∞	3.53[3]	22	–20
DWNT (3,0)@(6,0)	10.1	19.8	3.54	34	–11
DWNT (6,0)@(9,0)	19.6	30.7	3.54	31	–12
DWNT (4,0)@(8,0)	13.8	25.0	3.55	33	–10
DWNT (8,0)@(12,0)	27.9	38.6	3.55	31	–11
γ-V_2O_5 without layer rotation (see the text)					
Double layer	∞	∞	3.54[4]	20	–23
DWNT (3,0)@(6,0)	10.0	20.8	3.55	31	–11
DWNT (6,0)@(9,0)	21.3	30.2	3.55	29	–13
DWNT (4,0)@(8,0)	13.9	26.0	3.54	35	–7
DWNT (8,0)@(12,0)	28.1	38.7	3.55	30	–12
γ-V_2O_5 with layer rotation (see the text)					
Double layer	∞	∞	3.55[5]	26	–15
DWNT (3,0)@(6,0)	10.5	19.4	3.55	29	–13
DWNT (6,0)@(9,0)	20.6	32.1	3.55	28	–15
DWNT (4,0)@(8,0)	13.8	25.8	3.54	33	–8
DWNT (8,0)@(12,0)	26.0	37.9	3.54	30	–12

[1] D is the average diameter of inner (in) and outer (out) walls of DWNT estimated as the sum of radial distances to outmost and innermost oxygen atoms, t is the translational period.

[2] E_{form} is the formation energy and E_{int} is the interaction energy of SWNT (see Eq. (2)).

[3] The optimized lattice parameters of α-V_2O_5 double layer are a = 11.35 Å, b = 3.53 Å.

[4] The optimized lattice parameters of γ^*-V_2O_5 double layer are a = 11.25 Å, b = 3.54 Å.

[5] The optimized lattice parameters of γ-V_2O_5 double layer are a = 10.03 Å, b = 3.55 Å.

The structure of adhesion regions of γ^*-DWNTs is close to this phase. To get the structure more similar to the parent γ-V_2O_5 bulk, it is necessary to rotate every next nearest γ^*-layer by 180° around the normal to the layer plane. In that way one can get the centered orthorhombic $Cmc2_1$ (36) γ^{**}-V_2O_5 bulk phase (Fig. 5, left side, and Table 3). This phase resembles the structure of adhesion regions of γ-DWNTs in the case of Δn = 3. In principle, the γ^{**}-V_2O_5 phase can transform into γ-V_2O_5 with doubling of the unit cell because the space groups *Pnma* and $Cmc2_1$ have the common subgroup $Pmc2_1$ (26).

The formation energy of γ^{**}-V_2O_5 is about 8 kJ/mol. Thus, this phase is less stable than α-V_2O_5, but is more stable than γ-V_2O_5 (see Table 1). Unexpectedly, calculations give the close to zero formation energy of the γ^*-V_2O_5 phase, i. e. the stability of this phase is the same as that of the most stable phase α-V_2O_5.

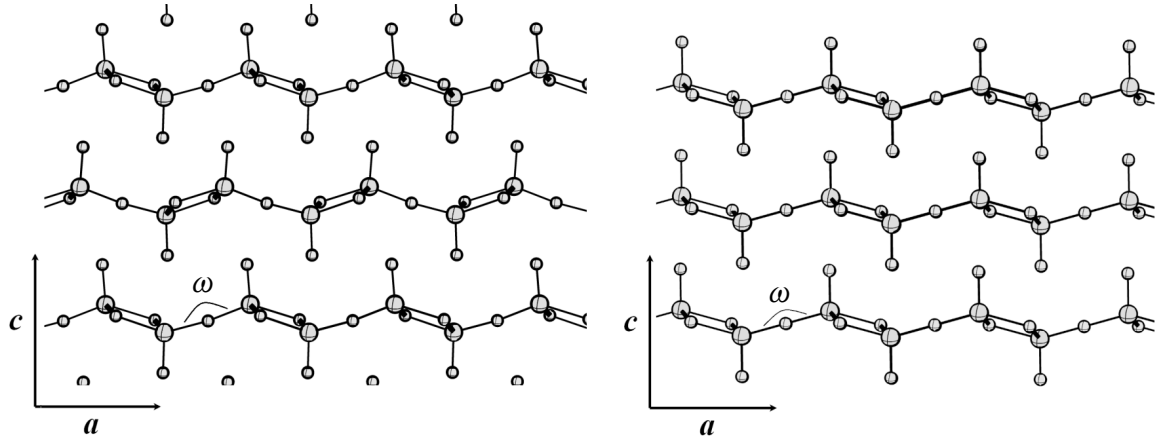

Fig. 5. The structures of the bulk crystal of γ^{**}- and γ^*-V_2O_5 phases are presented at left and right sides, respectively. The bridging V-O-V angles ω are equal to 180° and 173.5° for γ^*- and γ^{**}-V_2O_5, respectively. For optimized cell parameters and atomic positions see Table 3. V, large balls; O, small balls.

Table 3. The optimized crystal structure of γ^*-V_2O_5 and γ^{**}-V_2O_5.

	x/a	y/b	*z/c*
γ^*-V_2O_5, *Cm*/211 (12)[1]			
V	0.15	0	0.11
O(1)	0	0	0
O(2)	0.18	1/2	0.01
O(3)	0.14	0	0.47
γ^{**}-V_2O_5, *Cmc*2_1 (36)[2]			
V(1)	0	0.01	0.06
V(2)	–1/2	0.21	–0.06
O(1)	0	0.17	–0.01
O(2)	–1/2	0.04	0.01
O(3)	0	–0.15	0.01
O(4)	0	0.01	0.23
O(5)	1/2	0.22	–0.23

[1] γ^*-V_2O_5 cell parameters: a = 11.42 Å, b = 3.53 Å, c = 4.35 Å, β = 90.2°.

[2] γ^{**}-V_2O_5 cell parameters: a = 3.53 Å, b = 11.22 Å, c = 9.13 Å.

In order to investigate vibrational stability of the considered hypothetical phases, the phonon spectra were calculated at Γ-, *R*-, *Z*-points and at Γ-, *R*-points of BZ of γ^*-V_2O_5, and γ^{**}-V_2O_5 phases, respectively. Frequencies of the phonon modes at the considered BZ points are all positive thus confirming the stability of both hypothetical phases.

The literature search allows us to find that γ^*-V_2O_5 is isostructural to one of the metastable phases of niobium pentoxide *R*-Nb_2O_5 [27]. Note that niobium is the higher homologue of vanadium in the periodic table. Furthermore, the vanadium compound with the atomic structure very close to that of γ^*-V_2O_5 was experimentally found before. This is the mixed oxide of vanadium and molybdenum crystallized as monoclinic *C*2 (5) $(V_{0.7}, Mo_{0.3})_2O_5$ [28]. The difference between the structure of this mixed oxide and that corresponding to *C*2/*m* is minor. The author of [28] found that the orthorhombic α-V_2O_5 phase begins to transform into the monoclinic *C*2 phase at a relatively small content of molybdenum (about 20%). It seems remarkable that almost fifty years later we found the footprint of such phase in V_2O_5 DWNT.

The structure of γ^{**}-V_2O_5 has also been mentioned in the literature. First, this phase is mentioned in Ref. [29] in the context of formation of bronze γ-LiV_2O_5. Second, the γ^{**}-V_2O_5 structure was found under geometry optimization of the bulk V_2O_5 with an increased unit cell volume in the very recent computational work [30] (see Fig. 7 of Ref. [30]).

Consequently, we can suppose that the discovered new polymorphs of V_2O_5 may really exist under certain conditions or at least can manifest themselves in various nanostructures.

6. Conclusions

Formation energies of DWNTs are close in all considered cases. This fact allows us to suppose the possibility of formation of different DWNTs.

The interaction between the walls of α- and γ-V_2O_5 DWNTs results in the formation of adhesion and puckering local regions. The structure of the adhesion region in α-DWNTs is close to the α-V_2O_5 bulk structure.

The optimized structure of the adhesion regions of both types of γ-V_2O_5 DWNTs differs from that of the parent γ-V_2O_5 bulk. It is shown that the obtained layer stacking in these areas corresponds to the structure of the new stable V_2O_5 polymorphs named in the article as γ^*-V_2O_5 and γ^{**}-V_2O_5. We found that the γ^*-V_2O_5 atomic structure is close to the structure experimentally observed in the $(V_{0.7}, Mo_{0.3})_2O_5$ crystal.

Acknowledgements

The authors acknowledge the financial support of Saint Petersburg State University (Grant 12.50.1566.2013) and assistance of the University Computer Center in the accomplishment of high-performance computations.

References

[1] Y. Wang, K. Takahashi, H. Shang, and G. Cao, Synthesis and electrochemical properties of vanadium pentoxide nanotube arrays, J. Phys. Chem. B **109**(8), 3085–3088 (2005).

[2] J.S. Bonso, A. Rahy, S.D. Perera, N. Nour, O. Seitz, Y.J. Chabal, K.J. Balkus Jr., J.P. Ferraris, and D.J. Yang, Exfoliated graphite nanoplatelets–V_2O_5 nanotube composite electrodes for supercapacitors, J. Power Sources **203**, 227–232 (2012).

[3] G. Gu, M. Schmid, P.-W. Chiu, A. Minett, J. Fraysse, G.-T. Kim, S. Roth, M. Kozlov, E. Muñoz, and R.H. Baughman, V_2O_5 nanofibre sheet actuators, Nature Mater. **2**, 316–319 (2003).

[4] C. Zhou, L. Mai, Y. Liu, Y. Qi, Y. Dai, and W. Chen, Synthesis and field emission property of $V_2O_5 \cdot nH_2O$ nanotube arrays, J. Phys. Chem. C **111**(23), 8202–8205 (2007).

[5] P.M. Ajayan, O. Stephan, P. Redlich, and C. Colliex, Carbon nanotubes as removable templates for metal oxide nanocomposites and nanostructures, Nature **375**, 564–567 (1995).

[6] R.A. Evarestov, *Theoretical Modeling of Inorganic Nanostructures. Symmetry and Ab-initio Calculations of Nanolayers, Nanotubes and Nanowires*, Springer Series in NanoScience and Technology (Springer, Berlin–Heidelberg, 2015).

[7] G. Zhu, Z. Qu, G. Zhuang, Q. Xie, Q. Meng, and J. Wang, CO oxidation by lattice oxygen on V_2O_5 nanotubes, J. Phys. Chem. C **115**(30), 14806–14811 (2011).

[8] J.M. Cocciantelli, P. Gravereau, J.P. Doumerc, M. Pouchard, and P. Hagenmuller, On the preparation and characterization of a new polymorph of V_2O_5, J. Solid State Chem. **93**(2), 497–502 (1991).
[9] M.B. Smirnov, E.M. Roginskii, V.Yu. Kazimirov, K.S. Smirnov, R. Baddour-Hadjean, J.P. Pereira-Ramos, and V.S. Zhandun, Spectroscopic and computational study of structural changes in γ-LiV_2O_5 cathodic material induced by lithium intercalation, J. Phys. Chem. C **119**(36), 20801–20809 (2015).
[10] N. Pinna, M. Willinger, K. Weiss, J. Urban, and R. Schlögl, Local structure of nanoscopic materials: V_2O_5 nanorods and nanowires, Nano Lett. **3**(8), 1131–1134 (2003).
[11] V.V. Porsev, A.V. Bandura, and R.A. Evarestov, Hybrid Hartree–Fock-density functional theory study of V_2O_5 three phases: Comparison of bulk and layer stability, electron and phonon properties, Acta Mater. **75**, 246–258 (2014).
[12] V.V. Porsev, A.V. Bandura, and R.A. Evarestov, *Ab initio* modeling of single wall nanotubes folded from α- and γ-V_2O_5 monolayers: structural, electronic and vibrational properties, CrystEngComm **17**(17), 3277–3285 (2015).
[13] V.V. Porsev, A.V. Bandura, and R.A. Evarestov, Theoretical study of α-V_2O_5-based double-wall nanotubes, ChemPhysChem **16**(14), 3007–3014 (2015).
[14] J.P. Perdew, K. Burke, and M. Ernzerhof, Rationale for mixing exact exchange with density functional approximations, J. Chem. Phys. **105**(22), 9982–9985 (1996).
[15] C. Adamo and V. Barone, Toward reliable density functional methods without adjustable parameters: The PBE0 model, J. Chem. Phys. **110**, 6158–6170 (1999).
[16] R. Dovesi, V.R. Saunders, C. Roetti, R. Orlando, C.M. Zicovich-Wilson, F. Pascale, B. Civalleri, K. Doll, N.M. Harrison, I.J. Bush, P. D'Arco, and M. Llunell, *CRYSTAL09 User's Manual* (University of Torino, Torino, 2010).
[17] R. Dovesi, R. Orlando, B. Civalleri, C. Roetti, V.R. Saunders, and C.M. Zicovich-Wilson, CRYSTAL: a computational tool for the *ab initio* study of the electronic properties of crystals, Z. Kristallogr. **220**, 571–573 (2005).
[18] M.F. Peintinger, D.V. Oliveira, and T. Bredow, Consistent Gaussian basis sets of triple-zeta valence with polarization quality for solid-state calculations, J. Comput. Chem. **34**(6), 451–459 (2013).
[19] S. Grimme, Semiempirical GGA-type density functional constructed with a long-range dispersion correction, J. Comput. Chem. **27**(15), 1787–1799 (2006).
[20] T. Bučko, J. Hafner, S. Lebègue, and J.G. Ángyán, Improved description of the structure of molecular and layered crystals: *Ab initio* DFT calculations with van der Waals corrections, J. Phys. Chem. A **114**(43), 11814–11824 (2010).
[21] A.V. Bandura, R.A. Evarestov, and S.I. Lukyanov, Structure reconstruction of TiO_2-based multiwall nanotubes: first-principles calculations, Phys. Chem. Chem. Phys. **16**, 14781–14791 (2014).
[22] H.J. Monkhorst and J.D. Pack, Special points for Brillouin-zone integrations, Phys. Rev. B **13**(12), 5188–5192 (1976).
[23] V. Shklover, T. Haibach, F. Ried, R. Nesper, and P. Novák, Crystal structure of the product of Mg^{2+} insertion into V_2O_5 single crystals, J. Solid State Chem. **123**(2), 317–323 (1996).
[24] R. Enjalbert and J. Galy, A refinement of the structure of V_2O_5, Acta Cryst. C **42**, 1467–1469 (1986).
[25] J.M. Cocciantelli, P. Gravereau, J.P. Doumerc, M. Pouchard, and P. Hagenmuller, On the preparation and characterization of a new polymorph of V_2O_5, J. Solid State Chem. **93**(2), 497–502 (1991).
[26] A. Ghosh, E.J. Ra, M. Jin, H.-K. Jeong, T.H. Kim, C. Biswas, and Y.H. Lee, High pseudocapacitance from ultrathin V_2O_5 films electrodeposited on self-standing carbon-nanofiber paper, Adv. Funct. Mater. **21**(13), 2541–2547 (2011).
[27] R. Gruehn, Eine weitere neue Modifikation des Niobpentoxides, J. Less Common Met. **11**(2), 119–126 (1966).
[28] L. Kihlborg, The crystal structure of $(Mo_{0.3}V_{0.7})_2O_5$ of *R*-Nb_2O_5 type and a comparison with the structure of V_2O_5 and V_2MoO_8, Acta Chem. Scand. **21**, 2495–2502 (1967).
[29] J. Galy, Vanadium pentoxide and vanadium oxide bronzes – Structural chemistry of single (S) and double (D) layer $M_xV_2O_5$ phases, J. Solid State Chem. **100**, 229–245 (1992).
[30] H.P. Beck and S. Kohaut, A DFT study on the correlation between topology and Bader charges: Part II, effects of compression and dilatation of V_2O_5, Solid State Sci. **43**, 1–8 (2015).

TEORINIS α- IR γ-V_2O_5 DVIGUBŲ SIENELIŲ NANOVAMZDELIŲ TYRIMAS

V.V. Porsev, A.V. Bandura, R.A. Evarestov

Sankt Peterburgo valstybinis universitetas, Rusija